Individual Split Au Square Ring for Surface Enhanced Raman and Hyper-Raman Scattering

RuXin ZHang
Nanjing University of Aeronautics and Astronautics
Chaoling Du (cldu@nuaa.edu.cn)
Nanjing University of Aeronautics and Astronautics https://orcid.org/0000-0001-7665-1991
Lu Sun
Nanjing University of Aeronautics and Astronautics
Wang XuRong
Nanjing University of Aeronautics and Astronautics
Xiang Li
Nanjing University of Aeronautics and Astronautics
MingXin Lei
Nanjing University of Aeronautics and Astronautics
DaNing Shi
Nanjing University of Aeronautics and Astronautics

Research Article

Keywords: Split Au square ring, Surface enhanced hyper-Raman scattering (SEHRS), Surface enhanced Raman scattering (SERS), Localized surface plasmon resonance (LSPR), Finite element method (FEM)

Posted Date: November 11th, 2021

DOI: https://doi.org/10.21203/rs.3.rs-922355/v1

Plasmonics
https://doi.org/XXXX/XXXX

Individual split Au square ring for surface enhanced Raman and hyper-Raman scattering

RuXin Zhang[1], ChaoLing Du[1,2,*], Lu Sun[1], WangXu Rong[1],Xiang Li[1], MingXin Lei[1], and DaNing Shi[1,2]

Received: xxxxxx/Accepted: xxxxxx

Abstract

In this paper, individual split Au square rings were numerically proposed as novel substrates for surface enhanced Raman and hyper-Raman scattering (SERS and SEHRS) simultaneously. The peak wavelengths of their localized surface plasmon resonances (LSPR) are revealed to fall in the near-infrared and visible light region, respectively, which are able to be finely tuned to match well with the wavelengths of the incident laser and hyper Raman scattered light beams. Their SEHRS and SERS performances along with electromagnetic (EM) field distributions are numerically investigated by finite element method. With the enhancement of near electric-fields generated by LSPRs, the maximum SEHRS and SERS enhancement factors are demonstrated to reach 1.22×10^{12} and 10^{8}, respectively. Meanwhile, the corresponding SERS based refractive-index (RI) sensitivity factor reaches as high as 258nm/RIU and 893nm/RIU, at visible and near-infrared wavelengths, respectively. The proposed structure is believed to hold great promise both for developing SEHRS, SERS and SERS based RI sensing substrates, which shows strong potential applications in nano sensing and enhanced Raman scattering.

Keywords: Split Au square ring, Surface enhanced hyper-Raman scattering (SEHRS); Surface enhanced Raman scattering (SERS); Localized surface plasmon resonance (LSPR); Finite element method (FEM)

Introduction

As a two-photon excitation analogue of surface enhanced Raman scattering (SERS), surface enhanced hyper Raman scattering (SEHRS) has found fascinating applications in plasmon based bio/chemical molecule sensing and detection [1] as that of SERS [2]. This benefits from the excitation of localized surface plasmon resonance (LSPR), which is accompanied by significantly enhanced near electromagnetic (EM) fields. Compared to SERS, SEHRS gets most of SERS characteristics, but gets larger sensitivity to surface environmental changes and stronger EM field enhancements due to its nonlinearity of excitation [1, 3-6]. Under incidence, the two photons with the same frequency of ν are inelastically scattered from a ground state to a virtual state with

E-mail: cldu@nuaa.edu.cn

[1]College of Science, Nanjing University of Aeronautics and Astronautics, Nanjing 211100, PR China

[2]Key Laboratory of Aerospace Information Materials and Physics, Ministry of Industry and Information Technology, Nanjing 210016, China

energy of $2\nu \pm \nu_{vib}$, which corresponds to the Stokes and anti-Stokes scattering of hyper Raman scattering (HRS), respectively. Herein, ν_{vib} is the vibration frequency of adsorbed bio/chemical molecules [7]. Benefited from the development of SEHRS, the weak signals of HRS are able to be significantly amplified, whose enhancement factor (G_{SEHRS}) has been experimentally and/or theoretically reported to reach as high as 10^{13} [8-9]. Similar to SERS, by absorbing bio/chemical molecules on the surface of noble metal nanoparticles, strongly enhanced near electric-fields will be generated with the excitation of their LSPR, further enhances the weak HRS signals of molecules. By ignoring chemical enhancement and taking the EM enhancement to be the dominant enhancement mechanism, the enhancement factor of SEHRS can be estimated by

$$G_{SEHRS}^{EM} = \left|E(\nu)/E_0(\nu)\right|^4 \left|E(\nu_s)/E_0(\nu_s)\right|^2 = \left|g(\nu)\right|^4 \left|g(\nu_s)\right|^2 \quad (1)$$

Herein, $\left|E(\nu)/E_0(\nu)\right|^4$ and $\left|E(\nu_s)/E_0(\nu_s)\right|^2$ are the enhancements of the localized electric fields at ν and ν_s ($\nu_s = 2\nu - \nu_{vib}$), respectively. To access efficient SEHRS substrates, the matching of frequencies or wavelengths between LSPR modes of noble metal nanostructure and that of both the incident laser and HRS light is anticipated. In the last two decades, the development of efficient SEHRS substrates are getting growing interest. Different kinds of Ag nanostructures, such as nanowires [12], nanodimers [13], nanorices [15], nanocavities [16], nanorice multimers[17], etc [9,11,14] have been developed. Yet, SEHRS reports about Au nanostructure substrates are still limited in literature to the best of our knowledge. The SEHRS enhancement of spherical gold nanoparticles and nanorods has been reported to get 10^7 in 2018 [18]. In 2019, Madzharova et al. compared the SEHRS performances of silver and gold nanocavities, and highlighted the better stability under laser excitation of gold [19]. It is interesting to design appropriate gold nanostructures to access as high as G_{SEHRS} and simultaneously take the advantage of gold stability under laser excitation. It is also desirable to develop substrates working efficiently for SEHRS and SERS simultaneously. Compared to experiments, numerical simulation has proved to be an efficient method to deliver this [20].

Accordingly, in this work, individual split Au square rings were proposed to investigate the corresponding LSPR properties. Their extinction spectra and EM field distributions are numerically calculated by the finite element method (FEM), both of which are tuned as functions of the incident light wavelength, structure parameters, and polarization angles. The peak wavelengths of the LSPR of the optimized nanoparticle matche well with both the incident laser and HRS light. The corresponding G_{SEHRS} and G_{SERS} successfully demonstrate their strong potential applications in SEHRS and SERS simultaneously. In addition, their SERS based refractive index sensing performances are also discussed.

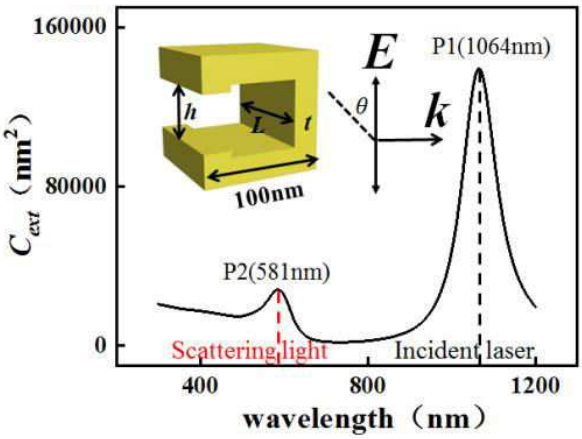

Figure 1. The typical FEM calculated C_{ext} spectra of the proposed split Au square ring. The upper-left inset illustrates the incident light configuration and schematic geometry of the proposed split Au square ring.

Structures and simulations

The upper-left inset of Figure.1 schematically presents the structural diagram of the concerned individual split Au square rings along with the incident light configuration. The extinction spectra and EM field distributions are then numerically simulated by the RF module of the commercial FEM package of COMSOL Multiphysics 4.1 (http://www.comsol.com). In our simulations for each concerned split Au square ring, the surrounding medium was assumed to be air, while the optical constants of Au is obtained from the experimental tabulated data of Johnson [21]. To avoid false reflections, a perfect matching layer has also been adopted surrounding the simulation domain, whose size is set to be $\lambda_{max}/2$ with λ_{max} being the maximum wavelength of the incidence. Meanwhile, the maximum meshing grid is set as $\lambda_{max}/8$ to confirm the convergence of the problem. After obtaining the EM field distributions, their absorption and scattering cross sections are then calculated by the following two equations.

$$C_{abs} = \frac{1}{I_0}\iiint P_{loss} dv \quad (2)$$

$$C_{sca} = \frac{1}{I_0}\iint (n \bullet S_{sca}) ds \quad (3)$$

Herein, I_0, $\boldsymbol{n}$, P_{loss} and $\boldsymbol{S_{sca}}$ refer to the normalized incident light intensity, the normal unit vector (pointing outward the split Au square ring), the power loss, and Poynting vector,

respectively. Then, the extinction cross section of each the concerned split Au square ring is calculated by summation its absorption and scattering cross sections.

Results and discussion

The multiple LSPR peaks and wide tunability of LSPR of the concerned nanoparticles promises their strong potential applications in both SEHRS and SERS. Fig. 1 shows the FEM calculated typical extinction spectra of the proposed split Au square ring with L =86 nm, h =49 nm, t =22 nm, θ=0º. It uncovers two obvious LSPR peaks, which locate at ~1064 and ~581nm, respectively. We label them as peak 1 (P1) and peak 2 (P2), which fall in the near-infrared region and visible light region, respectively. According to the EM enhancement mechanism of Eq(1), to achieve efficient SEHRS substrates, the peak positions of the two LSPR peaks are anticipated to match with both the incident laser and HRS wavelengths. Interestingly, the peak position of P1 just match well with the normally available SEHRS incident laser wavelength 1064nm in experiments. The corresponding scattered HRS light wavelength λ_s under 1064nm laser excitation is given by [15]:

$$\lambda_s = \frac{10^7}{\frac{10^7}{\lambda_{ex}/2} - \Delta\nu} \tag{4}$$

Herein, $\Delta\nu$ is HRS frequency shift of the adsorbed molecules with unit being cm^{-1}. The Raman frequency shift is chosen to be $1585cm^{-1}$ for discussion in this work, which is the dominant Raman shift of easily obtained molecule of pMBA [22]. Then, the corresponding λ_s is calculated to be ~581nm, which just match well with the peak position of P2 as illustrated of Fig.1. The corresponding G_{SEHRS} is predicted to reach as high as 1.22×10^{12}. It is comparable with G_{SEHRS} of Ag substrates reported elsewhere [4,15,24] and even larger than Au nanoparticle substrates reported in literature [18] as listed in Table 1. Hence, the proposed split Au square ring shows strong potential applications in SEHRS, which also shows the advantage of more stable than those of Ag counterparts.

Table 1. The G_{SEHRS} comparison between different substrates

Substrates	G_{SEHRS}
Split Au square ring (this work)	~10^{12}
Au nanosphere and Au nanorods[18]	~10^{7}
Ag disk[4]	~10^{8}
Al nanoantennas[4]	~10^{5}
Ag nanospheres[24]	~10^{9}
Ag nanorice[15]	~10^{9}
Mg_2N nanoantenna[25]	~10^{9}
Roughened Ag electrodes[9]	~10^{13}

The LSPR of split Au square ring can be finely tuned both by the geometry parameters of L, h and t, and by the polarization angle θ. Figure 2 shows some of the calculated typical extinction spectra. Figure. 2(a) demonstrates that the peak position of P1 (P2) decreases from 1097nm (594nm) at L=66nm to 1043nm (576nm) at L=106nm. Hence, P1 blue shift more with L increasing than that of P2. Similar response character is observed for the obtained peak wavelengths of P1 and P2 with respect to geometry parameters of t and h as demonstrated by Fig.2b-2c. Taking advantage of these geometry dependent multiple LSPR properties, one of these wavelengths is noted to be adjusted to match with the normally access laser wavelength of 1064nm in experiments.

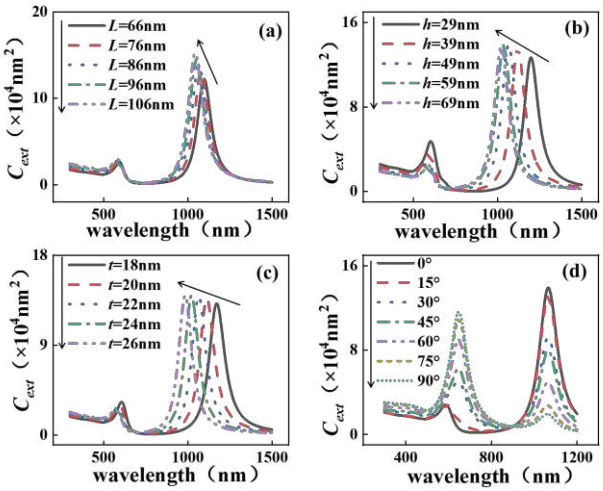

Figure 2. The FEM calculated L (a), h (b), t (c), and θ (d) dependent C_{ext} spectra of the proposed nanoring.

Hence, it paves the way for developing SEHRS substrates besides SERS. According to Eq (4), the corresponding HRS scattered wavelengths is able to be predicted for specific Raman frequency shifts of $\Delta\nu$ under specific laser wavelength excitation. Thanks to the develop of bottom-up nanoparticle fabrication, the split Au square ring with different structural parameters can be prepared by adjusting experimental conditions [23]. Therefore, the proposed split Au square ring can be used to simultaneously enhance both Raman and HRS signals. Herein, P1 and P2 is able to be tuned to 1064 and 581nm by adjusting L, h, and t, which shows simultaneously SERS and SEHRS strong potential applications. Yet, the LSPR properties of this substrate is also adjustable by the incident polarization angle θ as presented by Fig.2d. It reveals that the peak intensity of P1 gets weaken with θ increasing from 0° to 90° while that of P2 gets strengthen. However, the peak wavelength of P1 of this split Au square ring is not sensitive to θ, which shows neither blue nor red shift with θ varying. This is significant and advantageous both for SERS and SEHRS. A closer check of Fig.2d seems indicates that the polarization angle θ will tune P2 off the above-mentioned HRS wavelength, which is not desirable for SEHRS application. Yet, it is noted that P2 is asymmetric, which can be fitted well by two peaks

under different θ. Figure.3 shows some of the typical peak fitting results at θ=30°,45°,60°,90°, which reproduce the original spectra excellent at each θ. Interestingly, one of the fitted peak is insensitive to θ. Therefore, Fig.3 along with that of Fig.2d demonstrates that the peak positions of the two peaks at 1064nm and 581nm exhibit θ independent. This further confirms that the proposed split Au square ring with L =86 nm, h =49 nm, t =22 nm, and θ=0° serves as simultaneously excellent SERS and SEHRS substrate candidate.

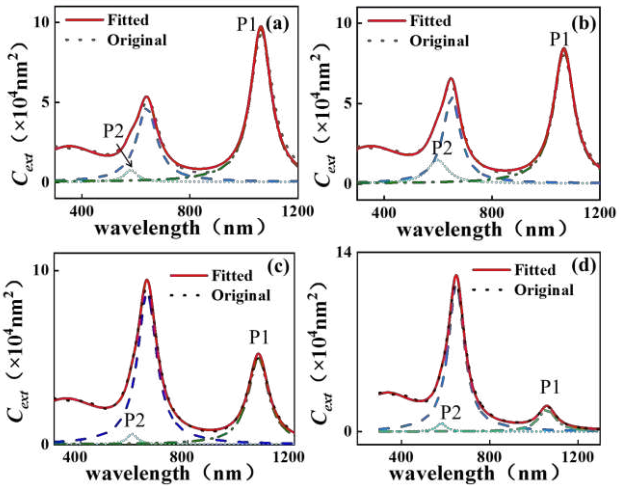

Figure 3. The obtained peak fitted C_{ext} spectra at θ=30°(a), 45°(b), 60°(c), 90°(d), respectively.

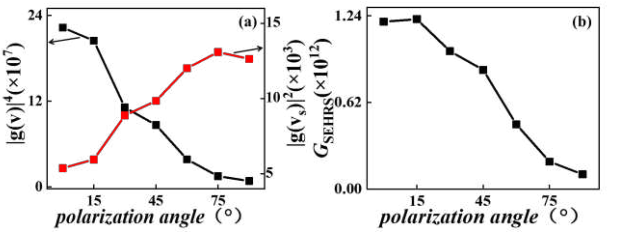

Figure 4. The FEM calculated enhancements of $|g(v)|^4$ and $|g(v_s)|^2$ (a), and G_{SEHRS} under different polarization angles (b).

As EM enhancement is the dominant enhancement mechanism of SEHRS, the enhancement of SEHRS of the 1585cm^{-1} Raman mode of the optimized split Au square ring is then calculated with respect to θ. It is proportional both to the excitation enhancement ($|g(v)|^4$) and scattering enhancement ($|g(v_s)|^2$) and they are contributed by the LSPR resonances at ~1064nm and ~581nm, respectively. The obtained results of Fig.4 show that $|g(v)|^4$ decreases with the increase of θ, while $|g(v_s)|^2$ increases with the increase of the θ. The calculated G_{SEHRS} under different polarization angles are shown as Fig. 4(b), which is revealed to be sensitive to θ. It demonstrates that the maximum G_{SEHRS} of the proposed split Au square ring reaches as high as 1.22×10^{12} under θ=15°. As listed in Table 1, the predicted G_{SEHRS} of the split Au square ring herein is larger than that of the previously proposed Au substrates [18], which also exceeds some of Ag, Al and Mg_2N of based SEHRS substrates [4,15, 24-25]. The outstanding G_{SEHRS} further proves the excellent SEHRS capabilities of the optimized split Au square ring.

It is necessary to have two different LSPRs at the same position of the SEHRS substrate [26]. To further compare the SEHRS enhancement factor under the different polarization directions, the corresponding near $|E|$ distributions of the

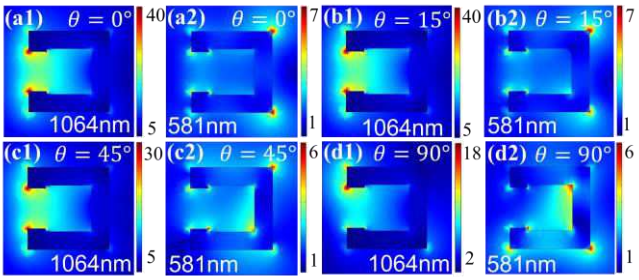

Figure 5. The FEM simulated typical $|E|$ distributions of the proposed nano structure.

split Au square ring under different polarization angles are simulated and the results are presented as Fig. 5. Fig.5(a1)-5(d1) reveals that the $|E|$ field around the opening gap region of the split Au square ring is significantly enhanced, especially around the opening two corners, serving as "hot spots" for SEHRS under the incidence of 1064nm. Meanwhile, $|E|$ at the gap region of the ring and all the ring corners is noted to be enhanced under excitation of the HRS scattered wavelength of 581nm as shown by Fig.5. This is greatly beneficial for the proposed ring application in SEHRS although it gets only ~5 fold increase compared to the incident electric field. It also provides multiple "hot spots" both at the inner ring gap region, outside surfaces and corners, which facilitates the EM signal enhancement for adsorbed molecules to be detected by SEHRS. With the increase of θ, the maximum $|E|$ at the LSPR wavelength of ~1064nm is simulated to gradually decrease, while the maximum $|E|$ at the LSPR wavelength of ~581nm gradually increases. It contributes to the above-mentioned θ dependent G_{SEHRS} response of Fig.4. The detailed $|E|$ distributions of Fig.5 also indicates that the molecules to be detected by SEHRS can be absorbed on both the inner and outer surfaces of the split Au square ring. It increases the adsorption area of the molecules to be detected and tends to increase the substrate efficiency for SEHRS as well.

The matching between the peak wavelength of the LSPR mode at 1064nm and the normally adopted laser in experiments also promises the potential candidate of the proposed nanoparticle for SERS and SERS based refractive index sensing. Similar to that of SEHRS, the enhancement

factor of SERS (G_{SERS}) is the crucial parameter to estimate SERS performance of the proposed substrate. Fig. 6 shows the FEM calculated G_{SERS} response of both LSPR peaks of P1 and P2 with respect to θ. Herein, G_{SERS} is taken to equal $|E|^4_{max}$, with $|E|^4_{max}$ being the obtained maximum enhanced electric field by ignoring chemical enhancement. The obtained G_{SERS} is revealed to exhibits similar changing character with respect to θ as illustrated in the left-y of Fig.4a. For P1, the obtained enhancement factor G_{SERS1}1 is revealed to reach maximum 2.23×10^8 at θ=0°, while G_{SERS2} reaches maximum 1.71×10^8 at θ=75°. The predicted enhancement factor is comparable for Au based SERS substrates reported elsewhere [27-28]. Yet, the proposed structure shows the advantage of working simultaneously at visible and near-infrared regions. Additionally, the refractive index (RI) sensitivity factor S of these two LSPR peaks are calculated as well, which is the key parameter to estimate the corresponding RI sensing performance of the concerned split Au square ring. In literature, S is defined as the derivative of the corresponding LSPR peak wavelength to the refractive index n of the surrounding medium [29-30]. Then, S of P1 and P2 are calculated to be 893 nm/RIU and 258 nm/RIU, respectively, which is comparable and even larger than other Au LSPR based sensors reported elsewhere [31-33]. Accordingly, besides SEHRS application, the excellent LSPR properties of the proposed split Au square ring contribute its excellent both SERS and SERS based RI sensing substrates in both visible and near-infrared light regions, which originates from the geometry and incident light configuration dependent electromagnetic field distributions.

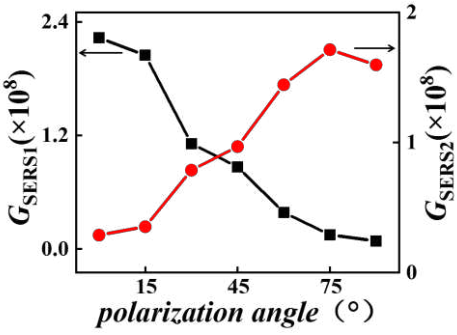

Figure 6. The FEM calculated responses of SERS enhancement factors (G_{SERS}) with respect to θ.

Conclusion

The LSPR properties of individual split Au square rings are numerically optimized to provide efficient substrates for simultaneously SEHRS and SERS applications. By tuning split ring geometry and incident light configuration, their multiple LSPR peaks are interestingly tuned to match both the incident laser and hyper Raman scattered light beams. The corresponding G_{SEHRS} is predicted to reach 1.22×10^{12} with L =86 nm, h =49 nm, t =22 nm, and θ=15°. It also provides excellent SERS substrate, which works simultaneously at visible and near-infrared regions and get maximum G_{SERS} 1.71×10^8 and 2.23×10^8 at visible and near-infrared regions, respectively. The obtained enhancement factors are even larger than some experimental report of Au/Ag nano substrates elsewhere and shows more stability than Ag. Its SERS based RI sensitivity factor is also predicted, which reaches 258nm/RIU and 893nm/RIU in the visible and near-infrared wavelengths, respectively. The present work paves the way for the development of new and efficient SEHRS , SERS and RI sensing substrates that can operate efficiently in both visible and near-infrared light regions.

Declarations

Funding This work was financially supported by Fundamental Research Funds for the Central Universities (No. NS2020057) and National Natural Science Foundation of China (Nos. 11774171 and 11874220).

Conflict of interest The authors declare no competing interests.

Availability of data and material All data included in this paper are available upon request by contacting the corresponding author.

Code availability Not applicable.

Author's contributions RuXin Zhang: Data curation and writing Lu Sun & WangXu Rong: Software and validation. ChaoLing Du: Supervision, review & editing. Xiang Li & MingXin Lei: Writing review & editing. DaNing Shi: Conceptualization and supervision.

Ethics approval Not applicable.

Consent to participate Not applicable.

Consent for publication Not applicable.

References

[1] Madzharova F, Heiner Z, Kneipp J (2017) Surface enhanced hyper Raman scattering (SEHRS) and its applications. Chem. Soc. Rev. 46: 3980-3999

[2] Pérezjiménez A I, Lyu D, Lu Z X, Liu G K, Ren B (2020) Surface-enhanced Raman spectroscopy: benefits, trade-offs and future developments. Chem. Sci 11: 4563-4577

[3] Milojevich C B, Mandrell B K, Turley H K, Iberi V, Best M D, Camden J P (2013) Surface-enhanaced hyper-Raman scattering from single molecules. J. Phys. Chem. Lett. 4: 3420-3423

[4] Butet J, Martin O (2015) Surface-enhanced hyper-Raman scattering: a new road to the observation of low energy molecular vibrations. J. Phys. Chem. C 119: 15547-15556

[5] Hulteen J C, Young M A, Duyne R V (2006) Surface-enhanced hyper-Raman scattering (SEHRS) on Ag film over nanosphere (FON) electrodes: surface symmetry of centrosymmetric adsorbates. Langmuir 22: 10354-10364

[6] Milojevich C B, Silverstein D W, Jensen L, Camden J P (2011) Probing two-photon properties of molecules: large non-condon effects dominate the resonance hyper-Raman scattering of rhodamine 6G. J. Am. Chem. Soc. 133: 14590-14592

[7] Denisov V N, Mavrin B N, Podobedov V B (1987) Hyper-Raman by vibrational exciations in crystals, glasses and liquids. Phys. Rep.151: 1-92

[8] Kelley, Myers A (2010) Hyper-Raman scattering by molecular vibrations. Annu. Rev. Phys. Chem. 61: 41-61

[9] Golab J T, Sprague J R, Carron K T, Schatz G C, Duyne R V (1988) A surface enhanced hyper-Raman scattering study of pyridine adsorbed onto silver: experiment and theory. J. Chem. Phys. 88: 7942

[10] Simmons P D, Turley H K, Silverstein D W, Jensen L, Camden J P (2015) Surface-enhanced spectroscopy for higher-order light scattering:a combined experimental and theoretical study of second hyper-Raman scattering. J. Phys. Chem. Lett. 6: 5067-5071

[11] Yu N T, Nie S, Lipscomb L A (1990) Surface-enhanced hyper-Raman spectroscopy with a picosecond laser. New vibrational information for non-centrosymmetric carbocyanine molecules adsorbed on colloidal silver. J Raman Spectrosc. 21(12): 797-802

[12] Leng W N, Yasseri A A, Sharma S, Li Z Y, Woo H Y, Vak D, Bazan G C, Kelley A M (2006) Silver nanocrystal-modified silicon nanowires as substrates for surface-enhanced Raman and hyper-Raman scattering. Anal. Chem. 78: 6279-6282

[13] Ikeda K, Mai T, Sawai Y, Nabika H, Uosaki K (2007) Hyper-Raman scattering enhanced by anisotropic dimer plasmons on artificial nanostructures. J Chem Phys 127(11): 111103-111103

[14] M Gühlke, Heiner Z, Kneipp J (2015) Combined near-infrared excited SEHRS and SERS spectra of pH sensors using silver nanostructures. Phys. Chem. Chem. Phys. 17: 26093-26100.

[15] Zhu S, Fan C, Pei D, Liang E, Hou H, Wu Y, (2018) Theoretical investigation of a plasmonic substrate with multi-resonance for surface enhanced hyper-Raman scattering. Sentific Reports 8(1): 1891

[16] Kim K H, Rim W S (2019) Slotted metal nanodisks supported by dielectric coated metallic substrates for ultrahigh enhancement of coherent anti-Stokes and hyper-Raman scattering. Applied Physics A. 125: 420

[17] Zhu S, Fan C, Liang E, Ding P, Dong X, Hao H (2021) Plasmon coupling nanorice trimer for ultrahigh enhancement of hyper-Raman scattering. Sci Rep 11: 1230

[18] Fani M, Zsuzsanna H, Jan S, Soeren S, Janina K (2018) Gold nanostructures for plasmonic enhancement of Hyper-Raman scattering. J. Phys. Chem. C. 122(5): 2931-2940

[19] Fani M, Denis Ö, João J, Wolfgang S, Janina K (2019) Plasmon enhanced two-photon probing with gold and silver nanovoid structures. Adv. Opt. Mater. 7: 1900650.

[20] Sungwoo L, Soohyun L, Jae-Myoung K, Jiwoong S, Eunbyeol C, Sungjae Y, Hajir H, Jwa-Min N, Sungho P (2021) Au nanolenses for near-field focusing. Chem. Sci. 12: 6355-6361

[21] Johnson P B, Christy R W (1972) Optical constants of the noble metals. Phys. Rev. B (Solid State) 6(12): 4370-4379

[22] Heiner Z, Gühlke M, Živanović V, Madzharova F, Kneipp J (2017) Surface-enhanced hyper Raman hyperspectral imaging and probing in animal cells. Nanoscale 9: 8024-8032

[23] Han P, Wayde M, Rolfe W E, Sarina S, Zhu H Y (2018) Metal nanoparticle photocatalysts: synthesis, characterization, and application. Part. Part. Syst. Charact 35: 1700489

[24] Mullin J, Valley N, Blaber M G, Schatz G C (2012) Combined quantum mechanics (TDDFT) and classical electrodynamics (Mie theory) methods for calculating surface enhanced Raman and hyper-Raman spectra. J. Phys. Chem. A 116(38): 9574-9581

[25] Kim K H, Wi J H, Choe M I (2020) Negative refraction in the visible and strong plasmonic resonances in photonic structures of the electride Material Mg_2N. ChemPhysChem 21(14): 1541-1547

[26] Zhang Y, Wen F, Zhen Y R, Nordlander P, Halas N J (2013) Coherent Fano resonances in a plasmonic nanocluster enhance optical four-wave mixing. Proc Natl Acad Sci U S A 110: 9215-9219

[27] Zhang P, Jie H, Ma X, Gong J, Nie Z (2013) Ultrasound assisted interfacial synthesis of gold nanocones. Chem Commun 49: 987-989

[28] Wang Y C, DuChene J S, Huo F, Wei W D (2014) An In situ approach for facile fabrication of robust and scalable SERS substrates. Nanoscale 6: 232-7236

[29] Khan A U, Zhao S, Liu G (2016) The key parameter controlling the sensitivity of plasmonic metal nanoparticles: aspect ratio. J. Phys. Chem. C 120(34): 19353-19364

[30] Fu T Y, Chen Y X, Du C L, Yang W C, Zhang R X, Su L, Shi D N. (2020) Numerical investigation of plasmon sensitivity and surface-enhanced Raman scattering enhancement of individual tin nanosphere multimers. Nanotechnology 31: 135210

[31] Lee S, Mayer K M, Hafner J H (2009) Improved localized surface plasmon resonance immunoassay with gold bipyramid substrates. Anal. Chem. 81: 4450-4455

[32] Zalyubovskiy S J, Bogdanova M, Deinega A, Lozovik Y, Pris A D, An K H, Hall W P, Potyrailo R A (2012) Theoretical limit of localized surface plasmon resonance sensitivity to local refractive index change and its comparison to conventional surface plasmon resonance sensor. J. Opt. Soc. Am. A 29: 994-1002

[33] Peixoto L, Santos J, Andrade G (2019) Plasmonic nanobiosensor based on au nanorods with improved sensitivity: a comparative study for two different configurations. Anal Chim Acta 1084: 71-77